Dynamical study of the transport properties of η-Mo$_4$O$_{11}$ single crystals by use of the photoinduced transient thermoelectric effect

M. Sasaki, G. X. Tai, S. Tamura, and M. Inoue

Department of Materials Science, Faculty of Science, Hiroshima University, Higashi-Hiroshima 724, Japan
(Received 30 March 1992; revised manuscript received 31 August 1992)

The pulsed-laser-induced transient thermoelectric effect (TTE) and the static transport properties (resistivity, Hall coefficient, magnetoresistance, and thermopower) of a quasi-two-dimensional η-Mo$_4$O$_{11}$ crystal have been measured over the time range 50 ns–2 ms and temperature range 4.2–300 K. The observed TTE voltages decay exponentially with time, showing relaxation processes with multiple relaxation times τ_i ($i = 1$–5) for thermal diffusions of photogenerated carriers (electrons and holes), from which we can evaluate the corresponding carrier mobilities μ_i. The temperature dependences of both dynamic and static transport quantities show anomalies around the characteristic temperatures $T_{c1} = 105$ K and $T_{c2} = 35$ K; T_{c1} is the well-known charge-density-wave (CDW) transition temperature, but for the latter no definitive x-ray evidence for a CDW transition is reported. However, using our dynamic data and the existing two-dimensional tight-binding model, together with our proposed nesting model of the Fermi surfaces and the CDW-related modifications of the electron and hole bands at T_{c1} and T_{c2}, we have self-consistently calculated the temperature dependence of the dc transport quantities, in satisfactory agreement with the experiments.

I. INTRODUCTION

Among various molybdenum oxides MoO$_{3-x}$ ($0 \leq x \leq 1$), the Magnéli phase crystal of monoclinic η-Mo$_4$O$_{11}$ has a quasi-two-dimensional (Q2D) structure, whose Fermi surfaces are known to be anisotropic in the b^*c^* plane elongated along the a^* axis, as predicted by recent band calculations using a two-dimensional tight-binding (block-band) model.[1] With such unique structural and electronic properties, this material undergoes a metal-semiconductor (or so-called Peierls) transition at $T_{c1} = 105$ K [and, possibly, at $T_{c2} = 35$ K (see later)] induced by charge-density-wave (CDW) instabilities, which are due to nesting of the Fermi surfaces of conduction electrons and holes with a nesting vector Q; only the nesting vector Q$=0.23$b* at T_{c1} is confirmed by diffuse x-ray scattering,[2] but to our knowledge there is no clear-cut x-ray evidence at T_{c2}. In an ideal one-dimensional (1D) system, such a nesting of the Fermi surface is complete, leading to a "CDW condensation" of the conduction carriers or to a "vanishing or nested" band of the original band that is produced by the CDW gap opening, while in the Q2D conductors, such as η-Mo$_4$O$_{11}$, a partial nesting occurs, which leads to both vanishing and "remaining" bands (see later).

Various static transport properties of η-Mo$_4$O$_{11}$ studied thus far have shown anomalies near T_{c1} and T_{c2} due to such conduction carriers in the remaining bands;[3–7] excellent reviews on these low-dimensional electronic properties have recently been given in Ref. 8, and by Canadell and Whangbo.[9] The latter has predicted that the possible Fermi surfaces of the remaining bands after the first CDW formation at T_{c1} are 2D "ellipselike pockets," which are further expected to undergo another nesting at T_{c2}, which hereafter is referred to as the second

CDW transition temperature, even though there is no direct evidence for this nesting vector. However, with these static data alone, one cannot discuss in detail the nature of the CDW-related band modifications at T_{c1} and T_{c2}.

Recently, we have developed a dynamic technique, called the "transient thermoelectric effect (TTE)" method, which enables us to obtain valuable information about conduction carriers, and have successfully applied it to various solids, such as semiconductors Si (Ref. 10) and GaAs,[11] intercalation compounds M_xTiS$_2$ ($M = 3d$ transition metals),[12] as well as high-T_c oxide superconductors;[13,14] preliminary experiments for η-Mo$_4$O$_{11}$ are reported earlier.[15] For a further understanding the CDW-related transport properties of η-Mo$_4$O$_{11}$, in the present work we have carried through the TTE and static measurements over a wide temperature range. With these experimental data, we have successfully performed self-consistent computer simulations of the static transport quantities by taking into account the possible nesting model of the Fermi surfaces based on the existing block-band model.[1,9,16] Such an attempt will provide us with valuable information about the CDW-related electronic properties of the Q2D carrier system of η-Mo$_4$O$_{11}$ below T_{c1}, and T_{c2} as well.

II. EXPERIMENTAL TECHNIQUES

The η-Mo$_4$O$_{11}$ crystals were grown by a chemical vapor transport technique.[6] The dc electrical resistivity, Hall effect, magnetoresistance using a potentiometric method, and TTE measurements were made along the b axis of the cleaved crystals (typically $2 \times 0.5 \times 0.1$ mm^3) over the temperature range 4.2–300 K. The experimental setup and measuring principle of TTE are described
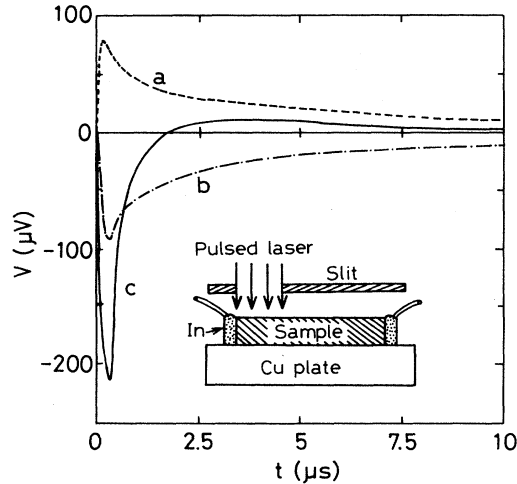
FIG. 1. Decay curves of the TTE voltages at (a) 200 K (dashed line), (b) 50 K (chain line), and (c) 4.2 K (solid line), where only the time range up to 10 μs is shown. The inset shows a pulsed laser irradiation through a slit (0.8 mm) upon one end of a crystal.

elsewhere.[10,15] A pulsed laser (laser power: ~ 1 J) produced by a Nd-doped glass laser source with a wavelength of 1.06 μm ($=1.17$ eV) and pulsewidth of 25 ns was irradiated normal to one end of a crystal through a slit of about 0.8 mm, as schematically shown in the inset of Fig. 1. Electrical contacts to both ends of the crystal were soldered by an indium metal. The laser-induced TTE voltage was detected over the wide time ranges 50 ns to 2 ms by a digital storage oscilloscope through a homemade preamplifier, whose output signal was fed to a computer for record and numerical analysis.

The laser intensity I at the sample position (illuminated area: about 0.8×0.5 mm^2) was controlled by an optical lens system and checked by a commercial fast-response joulemeter (Genetic Inc., Model ED-200). In the present experiments we have employed relatively weak laser intensity $I = 0.15 - 0.46$ mJ/cm^2 to avoid a thermal heating or bolometric effect of the laser light on the crystal. In fact, a rough evaluation of the photogenerated temperature rise ΔT under these laser illuminations using standard heat transport calculations shows that the values of ΔT are at most within a few Kelvin degrees, and the heat is dissipated within a short period (~ 100 ns) through a sample holder. Thus the observed decay curves of TTE voltages are primarily due to a thermal diffusion process of photogenerated carriers drifting along its concentration gradient in the sample.

III. EXPERIMENTAL RESULTS

Figure 1 shows the typical decay curves of the TTE signals at (a) $T = 200$ K ($T > T_{c1}$; normal state), (b) $T = 50$ K ($T_{c2} < T < T_{c1}$; first CDW state), and (c) $T = 4.2$ K ($T < T_{c2}$; second CDW state) for η-Mo$_4$O$_{11}$. Immediately after the laser-light irradiation, the TTE voltage V at the

normal state rises drastically to a positive value of about 100 μV within a short period (~ 50 ns), followed by exponential decays over the time range of about 50 μs with the characteristic relaxation times τ_1 and τ_2 to a constant negative value (-3 μV). The decay curves of observed TTE voltages at time t, $V(t)$, can be well expressed in the exponential form,

$$V(t) = V_0 + \Sigma a_i \exp(-t/\tau_i) \,,$$

where V_0 is a constant value at $t \to \infty$, a_i is the relaxation amplitude, and τ_i is the relaxation time for the ith relaxation process (or carrier type). Here it is interesting to note that the observed Hall coefficient R_H of this material is positive (see Fig. 3), but the static thermoelectric power S is negative over the wide temperature range 10–300 K and at liquid He temperatures it shows a sign reversal from negative to positive or vice versa with varying temperature (see Fig. 8). In view of these static data, the observed decay profile at the normal state is due to a thermal diffusion of conduction electrons. The induced TTE voltage at the first CDW state ($T_{c2} < T < t_{c1}$) is negative, which decays with other relaxation times τ_3 and τ_4 approaching zero at $t \to \infty$; in this case the decay process is regarded as due to a thermal diffusion of conduction holes. Furthermore, in the second CDW state ($T < T_{c2}$) the additional relaxation time τ_5 is observable, which is due to electrons.

In Fig. 2 is shown the temperature dependence of each relaxation time τ_i ($i = 1-5$) plotted in semilogarithmic scales. We note that the relaxation time τ_1 is observed over the whole temperature range, while τ_2 is observable
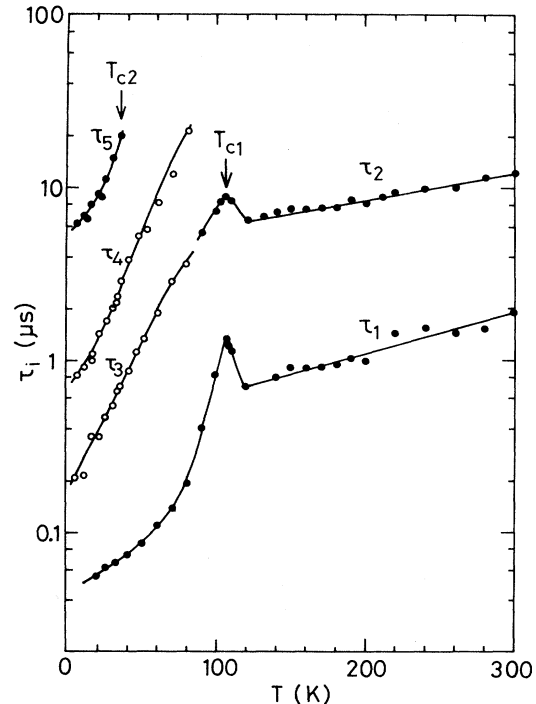

FIG. 2. Temperature dependence of the observed relaxation time τ_i ($i = 1-5$).

only at high temperatures $T > 100$ K, and that both τ_1 and τ_2 show anomalies near T_{c1}. The relaxation times τ_3 and τ_4 are observable below T_{c1}, while τ_5 is detectable only below T_{c2}. In Secs. V and VI, we shall evaluate the carrier mobilities self-consistently using these observed relaxation times.

Figure 3 shows the temperature dependences of (a) the observed electrical resistivity ρ and (b) Hall coefficient R_H measured at the magnetic field $B = 2$ T, indicated by open circles; solid, dashed, chain, and dotted lines are the calculated curves (see later). These transport quantities exhibit characteristic behaviors at two distinct temperatures T_{c1} ($= 105$ K) and T_{c2} ($= 35$ K). In particular, we should note that at low temperatures ($T < T_{c2}$) R_H is increased by four orders of magnitudes larger than that at the normal state ($T > T_{c1}$); as mentioned above, R_H is positive, while the static thermopower S is negative over the wide temperature range.

All of these experimental results indicate that there exist multiple conduction carriers of both electrons and holes in η-Mo$_4$O$_{11}$. With regard to the details of CDW-related electronic properties of this material system, however, much less can be drawn from these "static transport data" alone. To our knowledge, none has given detailed (in particular, quantitative) analyses of these properties thus far. In the present work, therefore, we have attempted to carry ou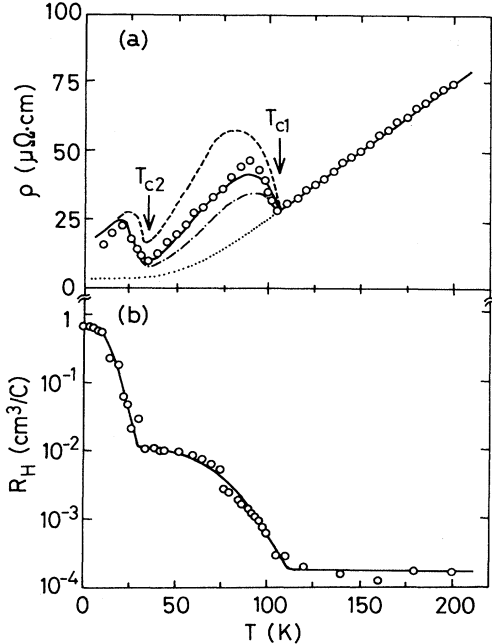t computer simulations of the static transport quantities using our "dynamic" TTE measurements, based on available theoretical predictions about the band and nesting models.[1,9,16] Since this material system consists of multiple carriers and their Fermi surfaces (which further undergo nesting after the CDW formation) that are not simple, a large number of parameters must necessarily be involved in the calculations. However, all these parameters can be determined self-consistently to reproduce all the experimental data.

IV. NESTING AND BAND MODELS

First it should be noted that the temperature range, over which each relaxation time is observable, is limited; the relaxation time τ_1 is observable over the whole temperature range and τ_2 is detected down to near T_{c1}, while τ_3 and τ_4 come into play in the CDW states ($T < T_{c1}$) and τ_5 solely below T_{c2} (Fig. 2). Taking into account the sign of the Hall coefficient, static thermopower, as well as TTE voltages, we have already made a tentative assignment of each relaxation time τ_i ($i = 1$–5) to each carrier type.[15]

Now, before computer simulations, we shall consider a possible nesting model and a band scheme of η-Mo$_4$O$_{11}$ based on the block-band model by Canadell and co-workers.[1,9,16] Figure 4(a) shows the schematic 2D Fermi surfaces of combined electron and hole pockets in the extended Brillouin-zone scheme proposed by them. Here, the electron pockets locate around the Γ point (which hereafter we denote by the e band) and along the Z-M

FIG. 3. (a) Temperature dependence of the observed electrical resistivity ρ (open circles) and the calculated curves using Eqs. (6), (11), and (12) with the nesting parameters $\beta_e = 0.70$ and $\beta_h = 0.78$ (solid lines; best-fit values), $\beta_e = 0.70$ and $\beta_h = 1.00$ (dashed line), and $\beta_e = 0.50$ and $\beta_h = 0.78$ (chain line); the dotted line is the theoretical one according to Eq. (11) alone (see text). (b) Temperature dependence of the observed Hall coefficient R_H measured at the magnetic field $B = 2$ T.
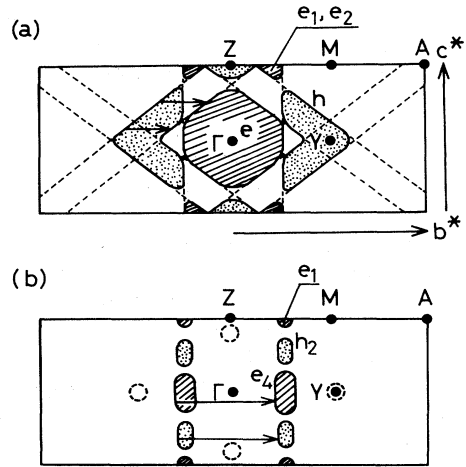

FIG. 4. (a) Schematic representation of two-dimensional electron (shaded area) and hole (dotted area) Fermi surfaces in the extended Brillouin-zone scheme for η-Mo$_4$O$_{11}$ at the normal state ($T > T_{c1}$) based on the block-band model by Canadell and co-workers (Refs. 1 and 9); dashed straight lines show the "hidden" 1D Fermi surfaces proposed by Whangbo and co-workers (Refs. 9 and 16) and arrows indicate the nesting vector **Q** for the first CDW transition. (b) Proposed remaining electron and hole Fermi surfaces after the first CDW transition ($T < T_{c1}$), where arrows show the expected nesting vector **Q'** ($= 2$**Q**) for the second CDW transition at $T = T_{c2}$; dotted circles show the hole h_3 or h_4 band (see text).

direction (e_1 and e_2 bands, corresponding to our TTE data, τ_1 and τ_2, respectively), while the hole pockets situate around the Y point (h band) and the Z point (Z pocket). In the normal state ($T > T_{c1}$), the carrier transport is mostly due to the e-band electrons and the h-band holes. The block-band model predicts that nesting of the Fermi surfaces occurs along the b^* axis with the magnitude $\mathbf{Q} = 0.25\mathbf{b}^*$. Furthermore, Canadell and co-workers[9,16] have proposed a concept of "hidden Fermi surface nesting" to explain the general CDW instabilities in low-dimensional metals, according to which real Fermi surfaces of CDW materials are composed of metallic 2D Fermi surfaces, such as described above (e and h bands), and several "hidden" 1D Fermi surfaces, as illustrated in Fig. 4(a) by dashed straight lines, where there are four parallel lines along the Γ-M direction and those along the Y-M direction, and two parallel lines along the Γ-Z direction.

According to their model of nesting at T_{c1}, the "V-shaped" portions in each "heart-shaped" hole surface (h band) are nested by the nesting vector $\mathbf{Q}$, and the remaining portions of the hole surfaces, except for those parallel to the Γ-Z direction, are also nested to the appropriate portions of the electron surface (e band) by $\mathbf{Q}$. This nesting is the most likely reason for the electronic instability at T_{c1} as confirmed by x-ray diffuse scattering.[2] Since the nesting in a Q2D system is incomplete, some portions of the Fermi surfaces remain unnested, leading to remaining bands lying along the Γ-Z direction, as indicated by solid lines in Fig. 4(b). In order to understand our TTE data, furthermore, we propose here additional hole pockets, which are supposed to locate somewhere near the Y and Z points, as indicated by dotted circles. In Fig. 4(b), we denote the electron pocket by the "e_1 band," corresponding to the relaxation time τ_1, and the hole pockets by the "h_3 and h_4 bands," corresponding to τ_3 and τ_4, respectively; at present we cannot give a definite assignment of the h_3 and h_4 bands to either of the dotted circles located at different points. As shown later, the other electron pocket (denoted by the e_4 band) and hole pocket (denoted by the h_2 band) also play an important role in the dc transport (see Sec. V), whose Fermi surfaces are expected to be strongly anisotropic (cylindrical shapes elongated along the a^* direction), even though the TTE signals cor-

responding to these e_4 and h_2 bands are undetected, probably because their relaxation amplitudes are too small.

On the other hand, the nesting vector at another transition temperature T_{c2} (where anomalies in various transport quantities are also observed) has not been confirmed by x-ray diffraction. This is probably because the weak satellites of x-ray diffuse scattering below T_{c2}, if any, will superimpose on the first satellites produced by nesting with the vector $\mathbf{Q}$ at T_{c1}, provided that the magnitude of the second nesting vector is $\mathbf{Q}' = 2\mathbf{Q}$ (indicated by arrows), as readily expected from Fig. 4(b). Even though there is no x-ray evidence, we assume here that the second CDW transition occurs at T_{c2} by nesting of the anisotropic e_4 and h_2 bands with $\mathbf{Q}'$, leading again to the nested and unnested (remaining) bands, as shown later (Fig. 5).

Based on the above nesting model modified slightly from the one by Canadell and Whangbo,[9] we propose the possible band scheme, as illustrated schematically in Fig. 5 (see also Table I): (a) In the normal state ($T > T_{c1}$), the holes in the h band around the Y point are filled up to the Fermi energy E_F^h and the electrons in the e band around the Γ point are up to E_F^e, just like a semimetal. These mobile electrons and holes with different carrier concentrations and mobilities contribute to the dc transport. The electrons in the e_1 and e_2 bands along the Z-M direction are responsible for the observed TTE signals with the relaxation times τ_1 and τ_2, respectively, but their contribution to dc transport is extremely small, because their carrier concentrations n_1 and n_2 are very low compared with those of the e and h bands (n and p, respectively) (see Table II). (b) In the first CDW state ($T_{c1} < T < T_{c2}$), the e band will split into the "nested" e_3 band with the first CDW gap energy $\Delta_1(T)$ and the remaining e_4 band, while the h band splits similarly into the nested h_1 band with $\Delta_1(T)$ and the remaining h_2, h_3, and, h_4 bands; the observed relaxation times τ_3 and τ_4 are due to the holes of the h_3 and h_4 bands, respectively, which may have small anisotropic (ellipsoidal) Fermi surfaces with large effective masses along the a^* axis. These electrons and holes in the remaining bands are responsible for dc conduction, while in the nested e_3 and h_1 bands only thermally excited carriers will contribute. (c)

TABLE I. Electron and hole bands (see Fig. 5) with carrier concentration and mobility, indicated by parentheses below, which contribute to the dc transport in the normal and CDW states of η-Mo$_4$O$_{11}$ (see text).

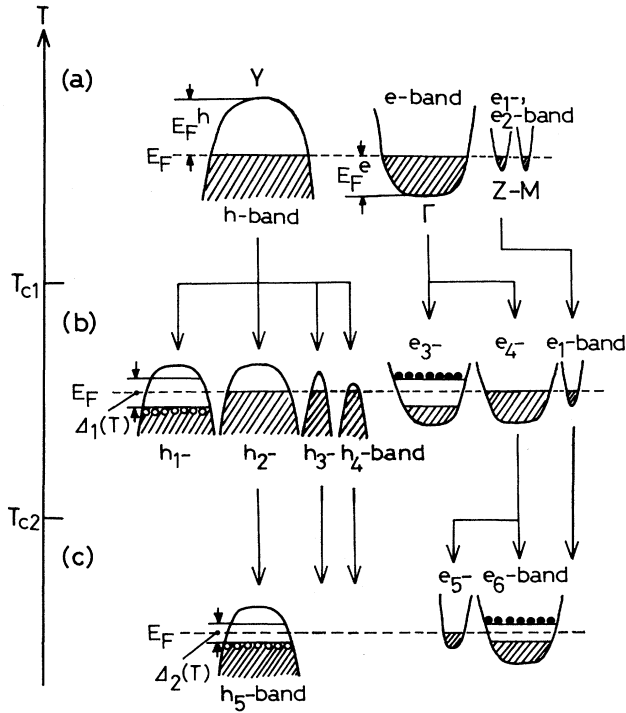| (a) Normal state ($T > T_{c1}$)	(b) First CDW state ($T_{c2} < T < T_{c1}$)	(c) Second CDW state ($T < T_{c2}$)
h band (p, μ_h)	h_1 band $[p_1(T), \mu_h]$	
	h_2 band (p_2, μ_h)	h_5 band $[p_5(T), \mu_h]$
	h_3 band (p_3, μ_3)	h_3 band (p_3, μ_3)
	h_4 band (p_4, μ_4)	h_4 band (p_4, μ_4)
e band (n, μ_e)	e_3 band $[n_3(T), \mu_e]$	
	e_4 band (n_4, μ_e)	e_5 band (n_5, μ_5)
		e_6 band $[n_6(T), \mu_e]$
e_1 band (n_1, μ_1)	e_1 band (n_1, μ_1)	e_1 band (n_1, μ_1)
e_2 band (n_2, μ_2)		

FIG. 5. Proposed band scheme for electrons and holes in η-Mo$_4$O$_{11}$; (a) normal state $(T > T_{c1})$, (b) first CDW state $(T_{c2} < T < T_{c1})$, and (c) second CDW state $(T < T_{c2})$ (see text).

In the second CDW state $(T < T_{c2})$, the e_4 band will be further decomposed into the remaining e_5 band (which is responsible for the observed τ_5) and the nested e_6 band with the second CDW gap energy $\Delta_2(T)$; similarly, the hole h_2 band is completely nested into the h_5 band with $\Delta_2(T)$. Thus the only remaining bands below T_{c2} are the e_1, h_3, h_4, and e_5 bands, corresponding to the observed

relaxation times τ_1, τ_3, τ_4, and τ_5, respectively.

Here we assume that in the CDW states, the remaining e_4 and h_2 bands have Q2D cylindrical Fermi surfaces [Fig. 5(b)], while the e_1, h_3, h_4, and e_5 bands have small ellipsoidal Fermi surfaces elongated along the a^* axis.

For numerical calculations of the dc transport quantities, we specify a carrier density and a mobility for each band by a simplified expression as listed in Table I; e.g., (p, μ_h) for the h band and (n, μ_e) for the e band. For simplicity, we assume that carrier mobilities in the Q2D nested and remaining bands are the same as those of the original bands. Moreover, the carrier mobility μ_i of the ith band $(i = 1-5)$ of the remaining electron or hole bands is evaluated from the observed relaxation times τ_i, and other quantities are determined semiempirically and self-consistently, as described later.

V. TRANSPORT QUANTITIES

A. Relaxation times and carrier mobilities

As discussed earlier,[10] the photoinduced TTE is essentially due to thermal diffusion process of conduction carriers from a high- to low-temperature region (or along a carrier concentration gradient) of a crystal, where the conduction carriers belong to their respective bands (Fig. 5). As found experimentally, the photoinduced TTE voltages decay exponentially with characteristic relaxation times τ_i, for which the theoretical analysis of the transport equation gives the following relation:[10]

$$\tau_i = L_i^2 / 2D_i , \tag{1}$$

where L_i and D_i are a diffusion length and a diffusion coefficient for the ith carrier pocket, respectively.

Since the electron and hole systems of η-Mo$_4$O$_{11}$ are degenerate, the relationship between D_i and carrier mobility μ_i is expressed in the modified Einstein relation as

TABLE II. Best-fit values of carrier concentrations, Fermi energies, and nesting parameters for electron and hole bands used for numerical calculations (see text).

	Band	Concentration (10^{20} cm^{-3})	Fermi energy (meV)	Nesting parameter
(a) Normal state	e band	$n = 30$	$E_F^e = 60$	
$(T > T_{c1})$	e_1 band	$n_1 = 0.0002$	$E_{F1}^e = 0.4$	
	e_2 band	$n_2 \sim 0$	$E_{F2}^e = 0$	
	h band	$p = 70$	$E_F^h = 140$	
(b) First CDW state	e_1 band	$n_1 = 0.0002$	$E_{F1}^e = 0.4$	
$(T_{c2} < T < T_{c1})$	e_3 band	$n_3(T)$		$\beta_e = 0.70$
	e_4 band	$n_4 = 9$		
	h_1 band	$p_1(T)$		$\beta_h = 0.78$
	h_2 band	$p_2 = 15$		
	h_3 band	$p_3 = 0.08$	$E_{F3}^h = 7.3$	
	h_4 band	$p_4 = 0.03$	$E_{F4}^h = 2.2$	
(c) Second CDW state	e_1 band	$n_1 = 0.0002$	$E_{F1}^e = 0.4$	
$(T < T_{c2})$	e_5 band	$n_5 = 0.12$	$E_{F5}^e = 2.2$	
	e_6 band	$n_6(T)$		
	h_3 band	$p_3 = 0.08$	$E_{F3}^h = 7.3$	
	h_4 band	$p_4 = 0.03$	$E_{F4}^h = 2.2$	
	h_5 band	$p_5(T)$		

$$D_i = (k_B \mu_i T/e)[F_{1/2}(\zeta_i)/F_{-1/2}(\zeta_i)] , \qquad (2)$$

where $F_{1/2}(\zeta_i)$ and $F_{-1/2}(\zeta_i)$ are the Fermi integrals with $\zeta_i = E_{Fi}/k_B T$ (E_{F_i} is the Fermi energy of the ith pocket). Thus we can evaluate μ_i from τ_i using the relation

$$\mu_i = eL_i^2/(2k_B \tau_i T)[F_{-1/2}(\zeta_i)/F_{1/2}(\zeta_i)] . \qquad (3)$$

Because we have no available data of L_i for η-Mo$_4$O$_{11}$, we have assumed that each diffusion length L_i is independent of the type of carriers, and their thermal diffusion processes are governed by the same scattering mechanism; thus we may put $L_i = L$. Here we use the following semiempirical relation found for a metallic intercalation compound, whose carrier concentrations are of comparable order of magnitude to those of η-Mo$_4$O$_{11}$ (10^{19}–10^{20} cm^{-3} (Ref. 6); $L = 1.3 \times 10^{-9} T^{1/3}/C$, where C is a slope of the ρ-T curve at high temperatures; in our case we have $C = 4.0 \times 10^{-7}$ Ω cm/K from Fig. 3(a).

Hereafter for clarity, we specify the physical quantities for the electron bands by the subscript i ($= 1$–6) and those for the hole ones by j ($= 1$–5) (see Table I); however, the carrier pockets of interest here are those corresponding to the relaxation times τ_1–τ_5, and thus $i = 1, 2,$ and 5, and $j = 3$ and 4.

Now we write the ratio of the Fermi energy E_{Fi}^e for the ith electron pocket with the carrier mobility μ_i, effective mass m_i^*, and electron concentration n_i in the CDW states to that for the original e band E_F^e as

$$E_{Fi}^2/E_F^e = (n_i/n)^{2/3}(m_e^*/m_i^*) , \quad (m_e^*/m_i^*)^\gamma = \mu_i/\mu_e , \qquad (4)$$

where n is the electron concentration and m_e^* is the effective mass of the original e band, and γ is a parameter characterizing a scattering mechanism; here we assume an acoustic-phonon scattering ($\gamma = \frac{5}{2}$).[11] Similarly, the ratio of the hole Fermi energy E_{Fj}^h for the jth hole band to that for the original h band E_F^h is written by

$$E_{Fj}^h/E_F^h = (p_j/p)^{2/3}(m_h^*/m_j^*) , \quad (m_h^*/m_j^*)^\gamma = \mu_j/\mu_h , \qquad (5)$$

where p_j is the hole concentration in the jth hole pocket with the effective mass m_j^*, while p is the hole concentration and m_h^* the effective mass of the h band.

B. Resistivity, Hall coefficient, and thermopower

The temperature dependences of the resistivity ρ, Hall coefficient R_H, and thermopower of the η-Mo$_4$O$_{11}$ crystal show drastic changes near T_{c1} and T_{c2}; correspondingly, the total carrier concentration p_H ($= 1/eR_H$) and the Hall mobility μ_H ($= |R_H/\rho|$) show similar behaviors. In this section we shall give functional forms to perform numerical calculations of various transport quantities using the dynamic data and the proposed band model.

1. Normal state

As mentioned earlier, in the normal state ($T > T_{c1}$) the large electron e band and hole h band are responsible for

the dc transport [Fig. 5(a)]; there are also small e_1 and e_2 bands which, however, will not contribute to the dc transport because their carrier concentrations n_1 and n_2 are negligibly low compared with n and p (see Table II). Employing such a two-carrier model for η-Mo$_4$O$_{11}$, we write the basic quantities, such as electrical resistivity ρ and Hall coefficient R_H, as given below:

$$\rho = 1/[e(p\mu_h + n\mu_e)] = 1/[ep\mu_h(1 + \alpha_1\alpha_2)] , \qquad (6)$$

$$R_H = [e(p\mu_h^2 - n\mu_e^2)]\rho^2$$
$$= (1/ep)(1 - \alpha_1\alpha_2^2)/(1 + \alpha_1\alpha_2)^2 , \qquad (7)$$

with $\alpha_1 = n/p$ and $\alpha_2 = \mu_e/\mu_h$ (electron charge $e > 0$). On the other hand, the thermopower S is given similarly by

$$S = S_h(1 - \alpha_1\alpha_2\alpha_3)/(1 + \alpha_1\alpha_2) , \qquad (8)$$

with $\alpha_3 = |S_e/S_h|$, where S_e and S_h are the e-band electron and h-band hole thermopowers, respectively, which can be written as

$$S_h = (\pi^2/3)(k_B^2/e)(\xi T/E_F^h) ,$$
$$S_e = -(\pi^2/3)(k_B^2/e)(\xi T/E_F^e) , \qquad (9)$$

since each carrier system is degenerate, where ξ is a dimensionless parameter characterizing a scattering process. Here we assume that in the normal state, where the observed ρ-T curve is linear [Fig. 3(a)], the carrier concentrations n and p (and thus the ratio α_1) are temperature independent and their mobilities μ_e and μ_h have the same temperature dependence, as $\mu_e, \mu_h \propto T^{-\gamma}$, where the exponent γ depends on a scattering mechanism. Thus the ratio α_2 is temperature independent; this is the case for α_3 from Eq. (9).

For calculations, we must know the values of the parameters α_1, α_2, and α_3. The ratio $\alpha_3 = |S_e/S_h|$ ($= E_F^h/E_F^e$) can be rewritten in the following form. Since the original electron and hole Fermi surfaces are assumed to be quasi-two-dimensional, their Fermi energies can be expressed as $E_F^e \propto n/m_e^*$ and $E_F^h \propto p/m_h^*$, and thus α_3 is reduced to

$$\alpha_3 = (p/n)(\mu_h/\mu_e)^{1/\gamma} = \alpha_1^{-1}\alpha_2^{-1/\gamma} . \qquad (10)$$

Since the resistivity ρ shows a metallic behavior in the normal state, we use the conventional Bloch-Grüneisen formula

$$\rho = \rho_R + C\theta_D(\theta_D/T)^{-5}$$
$$\times \int_0^{\theta_D/T} 4x^5 dx/[\exp(x) - 1][1 - \exp(-x)] , \qquad (11)$$

where ρ_R is a temperature-independent residual resistivity and θ_D is a Debye temperature. From Eq. (6), we obtain the carrier mobility μ_h and μ_e for the original h and e bands as

$$\mu_h = [ep\rho(1 + \alpha_1\alpha_2)]^{-1}$$

and

$$\mu_e = \alpha_2[ep\rho(1 + \alpha_1\alpha_2)]^{-1} ,$$

respectively, which can be evaluated by using Eq. (11) for ρ, together with the best-fit parameters ρ_R, θ_D, C, p, α_1, and α_2.

2. CDW states

According to the proposed model, the resistivity ρ_0 (at zero magnetic field $B=0$) and the thermopower S for the multiple carrier system in the CDW states can be expressed by the following forms:

$$\rho_0 = 1/e(\Sigma n_i\mu_i + \Sigma p_j\mu_j) , \tag{12}$$

$$S = \Sigma(\sigma_i S_i + \sigma_j S_j)/\sigma , \tag{13}$$

where the conductivity of each band is written by $\sigma_i = en_i\mu_i$ or $\sigma_j = ep_j\mu_j$ [$\sigma = \Sigma(\sigma_i + \sigma_j)$]. The thermopower S_i for the ith electron pocket and S_j for the jth hole pocket are evaluated by Eq. (9) with the Fermi energies E_{Fi}^e and E_{Fj}^h, respectively. Furthermore, taking into account the fact that the observed Hall coefficient R_H depends on a magnetic field B, we write the magnetic-field dependences of the Hall coefficient $R_H(B)$ {and thus the total carrier concentration $p_H(B)=1/[eR_H(B)]$ and the Hall mobility $\mu_H(B)=1/[e\rho p_H(B)]$} and transverse magnetoresistance by[17]

$$R_H(B) = 1/[ep_H(B)] = N/(A^2 + N^2 B^2) , \tag{14}$$

$$\Delta\rho/\rho_0 = [A/(A^2 + N^2 B^2) - \rho_0]/\rho_0 , \tag{15}$$

with

$$N = e[-\Sigma n_i\mu_i^2/(1+\mu_i^2 B^2) + \Sigma p_j\mu_j^2/(1+\mu_j^2 B^2)] ,$$

$$A = e[\Sigma n_i\mu_i/(1+\mu_i^2 B^2) + \Sigma p_j\mu_j/(1+\mu_j^2 B^2)] .$$

Here the numbers of thermally excited electrons ($i=3$ and 6) and holes ($j=1$ and 5) in the respective nested band can be expressed by the following expressions:

$$n_3(T) = n\beta_e\exp[-\Delta_1(T)/(k_B T)] ,$$

$$p_1(T) = p\beta_h\exp[-\Delta_1(T)/(k_B T)] ,$$

$$n_6(T) = n(1-\beta_e)\exp[-\Delta_2(T)/(k_B T)] , \tag{16}$$

$$p_5(T) = p(1-\beta_h)\exp[-\Delta_2(T)/(k_B T)] ,$$

where β_e and β_h ($0<\beta_e$, $\beta_h<1$) are regarded as the parameters representing the "degree of partial nesting" of the original e and h bands, respectively. Thus we may write the electron and hole densities of the remaining e_4 and h_2 bands in the forms

$$n_4 = n(1-\beta_e) \text{ and } p_2 = p(1-\beta_h) ,$$

respectively.

On the other hand, the temperature dependence of the first CDW gap energy $\Delta_1(T)$ is described by[7,18]

$$\Delta_1(T)/\Delta_1(0) = a_1 + [a_1^2 + b_1(1-T/T_{c1})]^{1/2} , \tag{17}$$

where $\Delta_1(0)$ is the gap energy at $T=0$, a_1 and b_1 are some constants. Here we use $(a_1^2+b_1)^{1/2}=3.5$ at $T=0$, as in a conventional BCS theory for normal superconductors. The best-fit value of the constants are $a_1 = 0.2$ and

$b_1 = 4.8$, which are obtained from the observed $\Delta_1(T)$-T curve;[7] similarly, the second CDW gap energy $\Delta_2(T)$ is also determined from the observed $\Delta_2(T)$-T curve determined by numerical analysis of the ρ-T curves.

VI. NUMERICAL CALCULATIONS AND DISCUSSIONS

A. Normal state

(1) The observed ρ-T curve in the normal state shown in Fig. 3(a) can be well represented by Eq. (11), as indicated by the solid line, with the best-fit values of $\rho_R = (2.0\pm1.0)\times10^{-6}$ Ω cm, $C = (4.0\pm0.1)\times10^{-7}$ Ω cm/K, and $\theta_D = (365\pm10)$ K; the evaluated value of θ_D is in good agreement with the reported one.[3]

(2) Using this calculated ρ-T curve and the observed (temperature-independent) total carrier concentration $p_H = 3.5\times10^{22}$ cm^{-3}, we can evaluate the temperature dependence of the Hall mobility $\mu_H(=1/e\rho p_H)$ as shown in Fig. 6(a) by solid line, which is in good agreement with the measured results.

(3) In order to calculate the thermopower and to obtain the carrier concentrations of the e and h bands, we need the values of independent parameters α_1 and α_2, which can be evaluated as follows: (i) Taking into account the sign of the Hall coefficient R_H and the thermopower S [see Eqs. (7)–(10)], we get the inequalities $\alpha_1 < 1$ and $\alpha_2 > 1$. (ii) Since in the unit cell of η-Mo$_4$O$_{11}$ there are four d electrons to form the Q2D e-band electron and h-band hole Fermi surfaces,[1,9] the sum of the carrier concentration ($n+p$) should not exceed the upper limit of these d electrons ($=1.4\times10^{22}$ cm^{-3}, calculated from the formula unit of η-Mo$_4$O$_{11}$ crystal), and it may be larger than, say, $\frac{1}{5}$, of this value; thus 3.0×10^{21} cm$^{-3} < (n+p) < 1.4\times10^{22}$ cm^{-3}. (iii) In addition, the electron and hole Fermi energies (E_F^e and E_F^h) are estimated to be of the order of 100 meV.[1] (iv) In order to satisfy these conditions (i)–(iii) and fit the calculated S-T
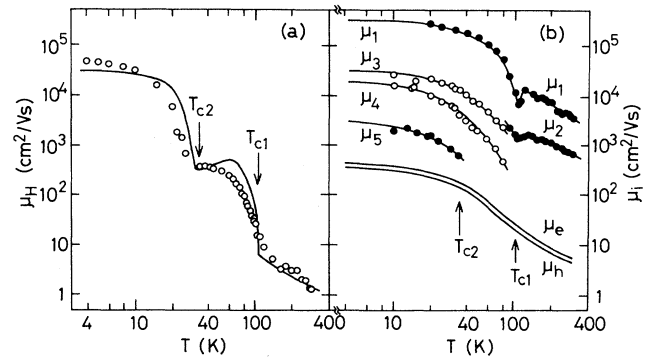

FIG. 6. (a) Temperature dependence of the observed Hall mobility μ_H (open circles) and the calculated one (solid line) using Eqs. (6), (7), (11), (12), and (14) with the best-fit parameters (Table II). (b) Temperature dependence of the carrier mobilities of electrons (μ_1, μ_2, and μ_5) and of holes (μ_3 and μ_4) determined self-consistently using the observed relaxation times τ_i ($i=1-5$) (Fig. 2); μ_e and μ_h are the calculated mobilities for the original e and h bands, respectively (see text).

curve with the observed one [Fig. 8(a)], self-consistent calculations of Eqs. (7)–(10) have been made repeatedly to get the following best-fit parameters: $\alpha_1 = 0.40 \pm 0.05$, $\alpha_2 = 1.2 \pm 0.1$, and thus $\alpha_3 = 2.3 \pm 0.3$ from Eq. (10) with $\gamma = \frac{5}{2}$.

(4) From these values, we readily obtain the values of carrier concentrations $n = (3 \pm 1) \times 10^{21}$ cm^{-3} for the e band and $p = (7 \pm 2) \times 10^{21}$ cm^{-3} for the h band from Eq. (7), the electron thermopower $S_e = -(330 \pm 130)$ and the hole one $S_h = (140 \pm 60)$ μV/K from the observed thermopower at 300 K ($S = -11$ μV/K) using Eq. (8), and the Fermi energies of the e and h bands $E_F^e = (60 \pm 20)$ and $E_F^h = (140 \pm 60)$ meV using Eq. (9) with $\xi = 3$,[19] respectively.

(5) The calculated temperature dependencies of the electron and hole mobilities μ_e and μ_h are shown in Fig. 6(b), which obey approximately the power law μ_e, $\mu_h \propto T^{-1}$, suggesting phonon scattering.

Furthermore, in order to examine whether the above values are reasonable or not, we have estimated the effective masses of the e and h bands, m_e^* and m_h^*, using the simple relations $E_F^e = h^2 \pi^2 (3n'/\pi)/8m_e^*$ and $E_F^h = h^2 \pi^2 (3p'/\pi)/8m_h^*$ for a Q2D system, where $n' = (n)^{2/3}$ and $p' = (p)^{2/3}$ in units of cm^{-2}. The calculation gives $m_e^* = (11 \pm 7)m_0$ and $m_h^* = (8 \pm 4)m_0$ (m_0: free-electron mass), which are reasonable orders of magnitude, compared to the reported value of $m^* \sim 10m_0$ for a 2D material system of high-T_c superconductors such as YBa$_2$Cu$_3$O$_{7-\delta}$.[20]

B. CDW states

Similarly, using the static and dynamic experimental data, we have carried through self-consistent calculations for the transport quantities and thermopower in the CDW states according to the following procedures:

(1) Since the relaxation time τ_2 corresponding to the e_2-band electron pocket becomes undetectable well below T_{c1} (Fig. 2), its carrier concentration n_2 can be neglected ($n_2 = 0$) in the CDW states, and thus we may put its Fermi energy $E_{F2}^e = 0$ or $F_{1/2}(\zeta_2)/F_{-1/2}(\zeta_2) = 1$ in Eq. (3). Thus, the corresponding carrier mobility μ_2 is evaluated using the relation $\mu_2 = eL^2/(2k_B T\tau_2)$ from Eq. (3).

(2) For the evaluation of other carrier mobilities μ_i from τ_i ($i = 1$ and 5), we must know the value of ζ_i for the Fermi integrals in Eq. (3). For this purpose, we first evaluate the initial value of μ_i with $\zeta_i = 0$ [or using the equation $\mu_i = eL^2/(2k_B T\tau_i)$]; a similar procedure is made to obtain μ_j for the jth hole band ($j = 3$ and 4).

(3) With these values of μ_i or μ_j and other adjustable parameters ($n_1, p_3, p_4, n_5, \beta_e$, and β_h), we calculate the dc transport quantities (ρ, p_H, μ_H, S, and $\Delta\rho/\rho_0$) using Eqs. (12)–(17) and compare them with the experimental data [Figs. 3(a), 6(a), 7(a), and 8].

(4) We get the Fermi energies E_{Fi}^e for the electron pockets and E_{Fj}^h for the hole pockets using Eqs. (4) and (5), from which we obtain new values of ζ_i and then μ_i (or ζ_j and μ_j for the hole bands).

(5) The numerical calculations of the procedures (3) and (4) are repeated until reasonable fits to the experi-
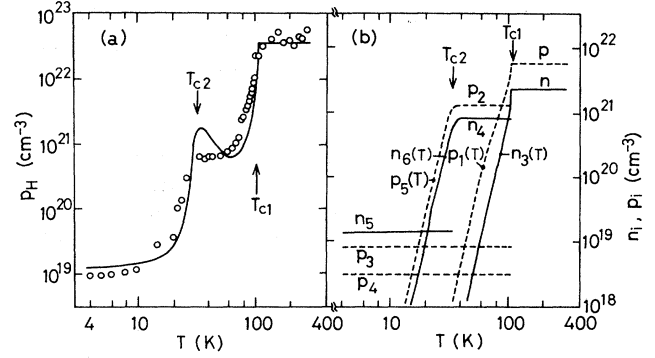

FIG. 7. (a) Temperature dependence of the observed carrier concentrations p_H ($= 1/eR_H$) (open circles) and the calculated one (solid line) using Eqs. (7) and (14) with the best-fit parameters (Table II). (b) Temperature dependence of the estimated carrier concentrations in each band (Table II), where solid lines show the carrier densities for electrons (n and $n_3 - n_6$) and dashed lines those for holes (p and $p_1 - p_5$), respectively (see text).

mental data are obtained.

From these computer calculations, according to the above procedure, we have obtained the best-fit values of the nesting parameters β_e and β_h, together with various quantities, such as carrier concentrations and Fermi energies of each electron and hole pocket, as compiled in Table II. It is particularly interesting to note that the nesting parameters introduced for the first time in the present work are determined to be $\beta_e = 0.70 \pm 0.02$ and $\beta_h = 0.78 \pm 0.02$, which in turn means that about 70% of the original e band and 78% of the original h band vanish (or nest) after the first CDW transition at T_{c1}, while the remaining e_4 band (30% of the original e band) and h_2 band (22% of the original h band) vanish completely after the second CDW transition T_{c2}. To our knowledge, thus
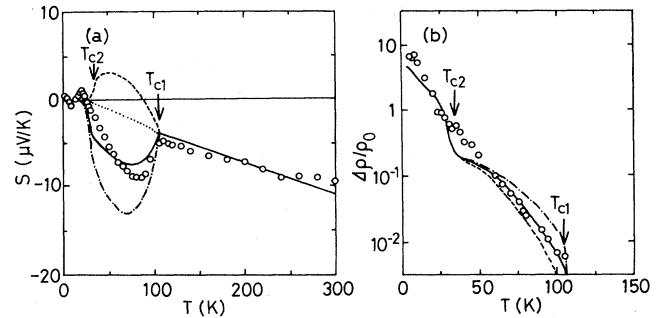

FIG. 8. (a) Temperature dependence of the observed thermopower S (open circles) and the calculated curves using Eqs. (8) and (13) with the nesting parameters $\beta_e = 0.70$ and $\beta_h = 0.78$ (solid line; best-fit values), $\beta_e = \beta_h = 0.70$ (dotted line), $\beta_e = 0.78$ and $\beta_h = 0.70$ (dashed line), and $\beta_e = 0.70$ and $\beta_h = 0.90$ (chain line). (b) Temperature dependence of the observed magnetoresistance $\Delta\rho/\rho_0$ at $B = 2$ T (open circles) and the calculated ones using Eq. (15) with the carrier concentration of the e_1 band $n_1 = 2 \times 10^{16}$ cm^{-3} (solid line; best-fit value), $n_1 = 0$ (dashed line), and $n_1 = 5 \times 10^{16}$ cm^{-3} (chain line).

far there has been no available information about the "degree of nesting" of the Fermi surfaces in 2D material systems; in this respect, we believe, the present work is of great significance.

The calculated curves obtained by the above procedure are shown by solid lines in the respective figures, which are all in satisfactory agreement with the experimental results [Figs. 3(a), 6(a), 7(a), and 8]. We have found that, in particular, the nesting parameters β_e and β_h affect strongly some physical properties, as shown in Fig. 3(a), for the resistivity ρ and in Fig. 8(a) for the thermopower S, where theoretical curves with different values of β_e and β_h are also illustrated by chain or dashed lines for comparison; one notices that in the case of equal amount of nesting of the original electron and hole pockets ($\beta_e = \beta_h$; dotted line), the thermopower S shows a linear temperature dependence over the whole temperature range. On the other hand, the electrons of the e_1 band with the extremely high mobility μ_1 [Fig. 6(b)] are found to influence significantly the transverse magnetoresistance $\Delta\rho/\rho_0$, as shown in Fig. 8(b) by dashed and chain lines; the best-fit value of n_1 is obtained to be $n_1 = (2\pm1)\times10^{16}$ cm^{-3}.

The temperature dependence of the carrier mobilities determined from the observed relaxation times (Fig. 2) is shown in Fig. 6(b) for the electron pockets (solid circles) and hole pockets (open circles). It should be noted that the observed value of the Hall mobility μ_H far below T_{c2} tends to approach those of μ_1 of the e_1 band electrons and μ_3 (and μ_4) of the h_3 (and h_4) band holes, which suggests that at low temperatures both conduction electrons and holes of these small remaining bands play an important role in the dc transport properties of η-Mo$_4$O$_{11}$. In the first CDW state the observed Hall mobility μ_H lies in the intermediate region between μ_e or μ_h, and μ_4-T curves, which indicates that the conduction electrons and holes of the e_4 and h_2 bands also contribute to the dc conduction; note that the mobility of the e_4 band is assumed to be equal to μ_e and that of the h_2 band to μ_h (Table I).

The experimental (open circles) and theoretical results (solid line) for the total carrier concentrations p_H are illustrated in Fig. 7(a). Except for the behavior near T_{c2}, the agreement between them is satisfactory. In Fig. 7(b) are shown the evaluated temperature dependence of carrier concentrations of each electron and hole band (see also Table II). We see that after the first CDW transition at T_{c1} the carrier concentrations of the original electron e band and hole h band are changed by 70% ($\beta_e = 0.70$) and 78% ($\beta_h = 0.78$) into the nested e_3 and h_1 bands, respectively. Below the second CDW transition temperature T_{c2}, the carrier densities of these conduction carriers are reduced drastically; these concentrations can be neglected at low temperatures, which means that nesting of the e_4 and h_2 bands is nearly complete below T_{c2}.

Finally, it is interesting to note that in this material system quantum oscillations (Shubnikov–de Haas) in the transverse magnetoresistance and Hall voltages have been observed at low temperatures $T < T_{c2}$; the fast-Fourier-transform analysis reveals that there are three main frequencies f_i (=4.5, 7.0, and 16 T).[7,21] According to the

present work, the observed three quantum oscillations are regarded as due to three different types of carrier pockets. As described above, the possible carriers responsible for them are the e_1 and e_5 band electrons, and the h_3 and h_4 band holes.

Using our best-fit values of these carrier concentrations n_i ($i = 1$ and 5) or p_j ($j = 3$ and 4) (Table II) we can evaluate the frequency f_i according to the following simple relation, with the cross-sectional area A_i and wave vector at the Fermi energy k_{Fi} in the b^*c^* plane for the ith electron pocket (the Fermi surface is assumed to be ellipsoidal shape in the limit of a very large mass along the a^* axis, as mentioned earlier),

$$f_i = h A_i / 4 e \pi^2 = h(\pi k_{Fi}^2)/4 e \pi^2 ,$$

where $2k_{Fi} = (3\pi^2 n_i)^{1/3}$; similar relations occur for the jth hole pocket with p_j. The calculated values of f_i are obtained to be $f_1 = 0.2$, $f_3 = 13$, $f_4 = 8$, and $f_5 = 17$ T for the e_1, h_3, h_4, and e_5 bands, respectively. Except for $f_1 = 0.2$ T, these values are in approximate agreement with the observed ones, which suggests that the observed quantum oscillations 4.5, 7.0, and 16 T are attributed to the holes in the h_4 and h_3 bands, and the electrons in the e_5 band, respectively. The quantum oscillation due to the e_1 band electrons has not been detected probably because of its extremely small Fermi surface. In view of these circumstances, we believe that our computer simulations based on the proposed nesting model and band scheme for the multiple carrier system of η-Mo$_4$O$_{11}$ are reasonable.

VII. CONCLUSIONS

Together with the static transport and thermopower experiments, the photoinduced TTE voltages have been measured for the Q2D η-Mo$_4$O$_{11}$ crystal over the time range 50 ns–2 ms and temperature range 4.2–300 K. The observed decay curves consist of multiple relaxation processes with the relaxation times τ_i ($i = 1$–5) for thermal diffusions of conduction carriers (electrons and holes), from which their carrier mobilities μ_i are evaluated self-consistently.

Based on the experimental results, as well as recent block-band models,[1,9,16] we have proposed a possible nesting model of the Fermi surfaces and a band scheme in the normal and CDW states of η-Mo$_4$O$_{11}$, as schematically shown in Figs. 4 and 5. In this material system, there exist primarily two types of mobile carriers (electrons in e band and holes in the h band) in the normal state, whose anisotropic Fermi surfaces locate around the symmetry points of the extended Brillouin zone. Due to CDW instabilities, each Fermi surface is subject to incomplete nesting at the transition temperature T_{c1}, leading to vanishing (or nested) and remaining bands.

According to these models, we have carried out self-consistent calculations for the dc transport quantities of this material consisting of multiple carriers, such as the resistivity ρ, Hall coefficient R_H, Hall mobility μ_H, total carrier concentration p_H, thermopower S, and magnetoresistance $\Delta\rho/\rho_0$. The simulated curves are all in good

agreement with the experimental data.

From the present studies, we have found that the observed relaxation times τ_1 and τ_2 are attributed to the electron e_1 and e_2 bands, respectively, but the electrons in the e_2 band do not contribute to the dc transport below T_{c1} because of very small carrier densities ($n_2 = 0$). Other relaxation times τ_3–τ_5 are observable solely below T_{c1}, among which τ_3 and τ_4 have been assigned to mobile holes in the h_3 and h_4 bands, respectively; τ_5 observed solely below T_{c2} is due to the remaining electron e_5 band.

Moreover, our numerical analyses have revealed that at the first CDW transition, about 70% ($\beta_e = 0.70$) of the original electron e band and about 78% ($\beta_h = 0.78$) of the hole h band vanish due to nesting of their Fermi surfaces, leading to the remaining electron e_4 band, and hole h_2, h_3, and h_4 bands, respectively; these bands have very small ellipsoidal Fermi surfaces with large effective masses along the a^* axis. At the second CDW transition,

the h_2 band is nested nearly completely. Ultimately, the remaining hole h_3, and h_4 bands and electron e_1 and e_5 bands contribute to the quantum (Shubnikov–de Haas) oscillations observed at low temperatures $T < T_{c2}$, their estimated frequencies being in reasonable agreement the observations. More confirmative experiments, as well as theoretical studies, with respect to the CDW-related band parameters for this Q2D material system are needed.

ACKNOWLEDGMENTS

[1]E. Canadell, M.-H. Whangbo, C. Schlenker, and C. Escribe-Filippini, J. Inorg. Chem. **28**, 1466 (1989).

[2]H. Guyot, C. Schlenker, J.-P. Pouget, R. Ayroles, and R. Roucau, J. Phys. C **18**, 4427 (1985).

[3]C. Schlenker, J. Dumas, C. Escribe-Filippini, H. Guyot, J. Marcus, and F. Fourcaudot, Philos. Mag. B **52**, 643 (1985).

[4]H. Guyot, C. Escribe-Filippini, G. Fourcaudot, K. Konate, and C. Schlenker, J. Phys. C **16**, L1227 (1983).

[5]M. Inoue, Y. Ueda, H. Negishi, M. Sasaki, T. Ohba, Y. Kitano, and Y. Komura, J. Less Common Met. **115**, 261 (1986).

[6]M. Inoue, S. Ôhara, S. Horisaka, M. Koyano, and H. Negishi, Phys. Status Solidi B **148**, 659 (1988).

[7]S. Ôhara, M. Koyano, H. Negishi, M. Sasaki, and M. Inoue, Phys. Status Solidi B **164**, 243 (1991).

[8]*Low-Dimensional Electronic Properties of Molybdenum Bronzes and Oxides,* edited by C. Schlenker (Kluwer Academic, Dordrecht, 1989), p. 159.

[9]E. Canadell and M.-H. Whangbo, Chem. Rev. **91**, 965 (1991).

[10]M. Sasaki, H. Negishi, and M. Inoue, J. Appl. Phys. **59**, 796 (1986).

[11]M. Sasaki, S. Horisaka, and M. Inoue, Jpn. J. Appl. Phys. **26**, 1704 (1987).

[12]M. Sasaki, M. Koyano, and M. Inoue, J. Appl. Phys. **61**, 2267 (1987).

[13]M. Sasaki, G. X. Tai, S. Tamura, and M. Inoue, Physica C **185-189**, 959 (1991); M. Sasaki, M. Koyano, H. Negishi, and M. Inoue, in *Science and Technology of Thin Film Superconductors 2,* edited by R. D. McConnel and R. Noufi (Plenum, New York, 1990), p. 517.

[14]M. Sasaki, G. X. Tai, S. Tamura, and M. Inoue, Phys. Rev. B **46**, 1138 (1992).

[15]M. Sasaki, G. X. Tai, and M. Inoue, Phys. Status Solidi B **162**, 553 (1990).

[16]M.-H. Whangbo, E. Canadell, P. Foury, and J.-P. Pouget, Science **252**, 96 (1991).

[17]N. P. Ong and P. Monceau, Solid State Commun. **26**, 487 (1978).

[18]M. Izumi, T. Iwazumi, K. Uchinokura, R. Yoshizaki, and E. Matsuda, Solid State Commun. **51**, 191 (1984).

[19]M. Koyano, H. Negishi, Y. Ueda, M. Sasaki, and M. Inoue, Phys. Status Solidi B **138**, 357 (1986).

[20]G. A. Thomas, J. Orenstein, D. H. Rapkine, M. Capizzi, A. J. Millis, R. N. Bhatt, L. F. Schneemeyer, and J. V. Waszczak, Phys. Rev. Lett. **61**, 1313 (1988).

[21]M. Koyano, S. Horisaka, H. Negishi, M. Inoue, T. Sakakibara, T. Goto, S. Takeyama, and N. Miura, Solid State Commun. **67**, 657 (1988).